

# Characterization of $\gamma$ -ray background at IMAT beamline of ISIS Spallation Neutron Source.

G. Festa<sup>1</sup>, C. Andreani<sup>1,2,3</sup>, L. Arcidiacono<sup>1,2,4</sup>, G. Burca<sup>5</sup>, W. Kockelmann<sup>5</sup>, T. Minniti<sup>5</sup>, R. Senesi<sup>1,2,3</sup>

1. Centro Fermi-Museo Storico della Fisica e Centro Studi e Ricerche “Enrico Fermi”, Rome, Italy
2. University of Rome Tor Vergata, Department of Physics and NAST Center, Rome, Italy
3. CNR-IPCF Sezione di Messina, Messina, Italy
4. UCL Institute of Sustainable Heritage, University College London, London, UK
5. STFC-Rutherford Appleton Laboratory, ISIS Facility, Chilton, OX11 0qx, UK

E-mail: giulia.festa@centrofermi.it

**Abstract.** The environmental  $\gamma$ -ray background on the IMAT beamline at ISIS Spallation Neutron Source, Target Station 2, is characterized via  $\gamma$  spectroscopy. The measurements include gamma exposure at the imaging detector position, along with the gamma background inside the beamline. Present results are discussed and compared with previous measurements recorded at INES and VESUVIO beamlines operating at Target Station 1. They provide new outcome for expanding and optimizing the PGAA experimental capability at the ISIS neutron source.

## 1. Introduction

In recent years, the use of neutron techniques at spallation neutron sources is rapidly expanding with applications spanning from the characterization of environmental  $\gamma$  signal at the neutron beamlines to the elemental analysis of materials and artefacts [1-3]. Spallation neutron sources provide intense flux of cold, thermal, epithermal and fast neutrons with energy ranging from meV to MeV. In most cases the  $\gamma$  signals measured at beamlines is produced by neutron interaction with the components along their flight path. The highest intensity signals originated from neutron capture reaction in the irradiated materials, i.e. flanges, beam-stop, sample holder and sample; furthermore,  $\gamma$  rays are produced by capture after scattering occurring in the beamline walls and detectors [1]. The neutron capture reaction is the consequence of a well-known process: the elemental nuclei irradiated by neutron beams capture neutrons producing excited compound nuclei that usually return to the ground state with a  $\gamma$  cascade with a multiplicity that depends of the target nucleus; the compound nucleus may be radioactive and unstable and may decay emitting delayed- $\gamma$  [4]. Prompt Gamma Activation Analysis (PGAA) measures the promptly emitted  $\gamma$  spectra during neutron irradiation, providing elemental analysis of the emitting nuclides. The intensity of the  $\gamma$  peaks being proportional to  $N/A$ , where  $N$  is the number of atoms per nuclide and  $A$  is the neutron-irradiated area [4-7]. The characterization of the  $\gamma$  signal provides unique information on the sources, which produce dose rate in the beamlines, and for the evaluation of the  $\gamma$  activation and radiation damage of the instrumentation. The latter piece of information becomes particularly relevant for those beamlines using imaging detectors, such as semiconductor devices (CCD and CMOS sensors) [8-10].

IMAT (Imaging and Materials Science & Engineering) [11-13] is the new imaging and diffraction instrument operating at the ISIS Spallation Neutron Source installed at Target Station 2 (TS2) with “friendly-user” program opened in October 2016. IMAT allows a unique combination of imaging and spatially resolved diffraction techniques, with capabilities in terms of non-destructively radiography and tomography reconstruction tailored to multipurpose studies such as neutron investigation in materials science and processing, engineering and cultural heritage [14-17]. The present study reports on a systematic characterization of environmental  $\gamma$  signal on IMAT in key configurations. A comparison of  $\gamma$  signal is discussed and compared with previous measurements performed on INES and VESUVIO beamlines installed on Target Station 1 (TS1) [1].

## 2. Experimental setup

IMAT is an instrument installed at Target Station 2, viewing a coupled liquid hydrogen moderator. Two are the IMAT special features: energy- dispersive neutron imaging [18] and the capability of combining neutron imaging and diffraction [12]. In particular, the instrument offers a combination of imaging and spatially resolved diffraction modes such as neutron radiography, neutron tomography, energy-dispersive neutron imaging, neutron strain scanning, crystallographic structure and phase analysis, texture analysis, and non-destructive testing. Neutron studies on IMAT find a broad range of imaging and diffraction applications ranging from aerospace and transportation, civil engineering, power generation to earth sciences, cultural heritage and agriculture. The neutron flight-path of the instrument is 56 m from moderator to sample, with large dimensions of the experimental area, ca. 5x6 m. A field of view (FOV) of 200x200 mm<sup>2</sup> can be obtained on the IMAT instrument with good uniformity of the neutron intensity. In the present study, FOV is set to 200x200 mm<sup>2</sup>. The beam dump, located at 4 m from the sample position is mostly composed by HR4 steel covered by borated wax (borated paraffin ~5 at% B). Neutrons scattered by the sample or other beamline components may hit the walls made of steel tanks filled by borated wax. The Camera Positioning System (CPS) frame is positioned after the sample position in the transmission direction and is composed of 6082-T6 aluminum alloy. The upstream window, made of 2014-T6 aluminum alloy, is 0.5 mm thick. IMAT is equipped with a fast imaging camera for radiographic and tomographic measurements. The aluminum camera box contains a neutron scintillator screen of <sup>6</sup>LiF/ZnS:Ag followed by an optical mirror composed by fused silica. The image reflected by the mirror is recorded by a test intensified CCD of 512 x 512 pixels. In the present experiment,  $\gamma$ -ray spectra are recorded using an ORTEC - GMX15 HPGe detector [19] with efficiency varying between 25% at 60 keV and 3-7% at 1332 keV. This kind of detector is resistant to damage by fast neutrons and can be used in a neutron environment. The HPGe detector is located at 1.5 m from the sample position; its entrance window is a 0.3  $\mu$ m-thick, ion-implanted contact, extending the lower range of energies to about 3 keV. The electronic chain of the data acquisition uses the ORTEC-DSPEC50 [19] as high voltage supply and multi-channel analyzer; pulse height spectra are acquired using the ORTEC MAESTRO MCA software [19]. Shaping parameters are 12  $\mu$ s for a rise time and fall time, 0.8  $\mu$ s for the flat top. The system is placed in the measurement position without shielding, and no Compton suppression is applied.

The experimental set-up used in the present study is shown in figure 1. Two kind of samples are chosen to show the influence of the irradiated materials in the sample position: an iron slab and a vanadium rod. The iron slab was used as an example of the influence of the presence of an iron-based metal on the  $\gamma$  signal at camera position and it is representative of the Fe-based alloys such as steel, often used in the engineering applications. Vanadium is chosen because it is an isotropic scatterer to show the effects of the gammas coming from the neutron capture after scattering by the walls. Iron and vanadium samples are located at the center of the instrument, at sample position, in order to perform  $\gamma$  measurements tailored to study the effects on the IMAT  $\gamma$  background. The iron sample is a slab with a square shape of 15 x 15 cm<sup>2</sup>, 18 mm thickness and vanadium sample is a cylinder, 4 mm diameter and 7 cm height.

A series of experiment runs, each 40 minutes long, are performed in four different configurations, namely:

- C1) IMAT environmental  $\gamma$  background (no sample in the beam) at the position of the  $\gamma$  sensitive detector without camera box;
- C2)  $\gamma$  background with an iron slab sample located at sample position (sample A);
- C3)  $\gamma$  background with a vanadium slab sample located at sample position (sample B);
- C4) IMAT environmental  $\gamma$  background at the position of the  $\gamma$  sensitive detector with camera box in place.

In particular, the configurations C2) and C3) are intended primarily to probe the modification to the background due to sample scattering, which is expected to increase the number of neutrons hitting the beamline layout components. As such C2) and C3) can provide a realistic insight on the effect of sample dependent background for structural materials which are among the main areas of the scientific program on IMAT.

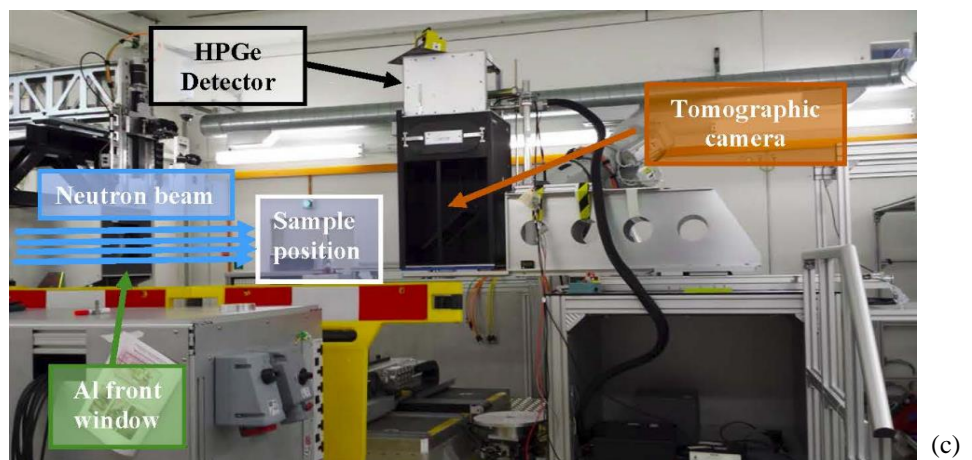
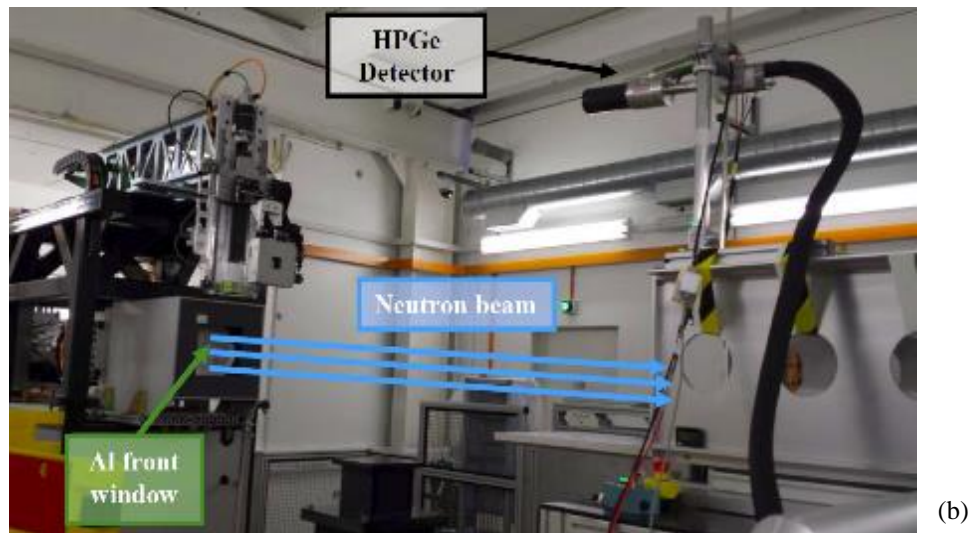
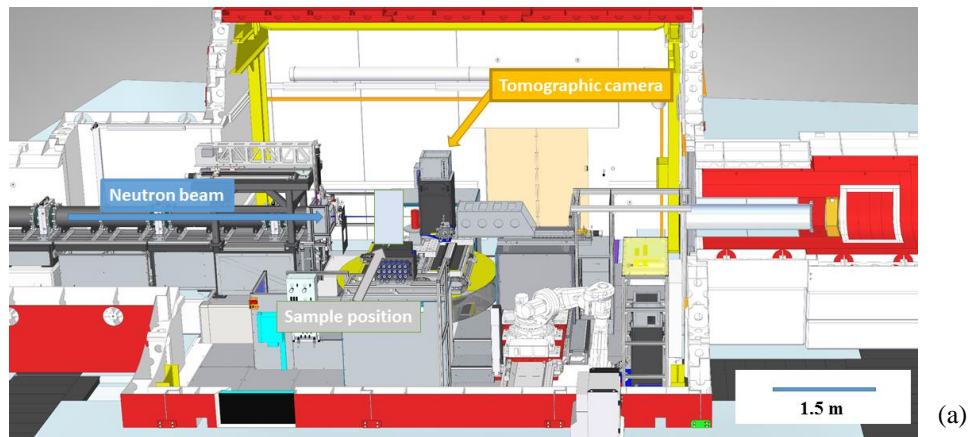


**Figure 1.** a) Schematic layout of IMAT beamline and the experimental setup used for  $\gamma$ -ray spectroscopy b) without the camera box and c) with the camera box.

### 3. Results and discussion

The environmental  $\gamma$  signal recorded at IMAT beamline is reported in figure 2.

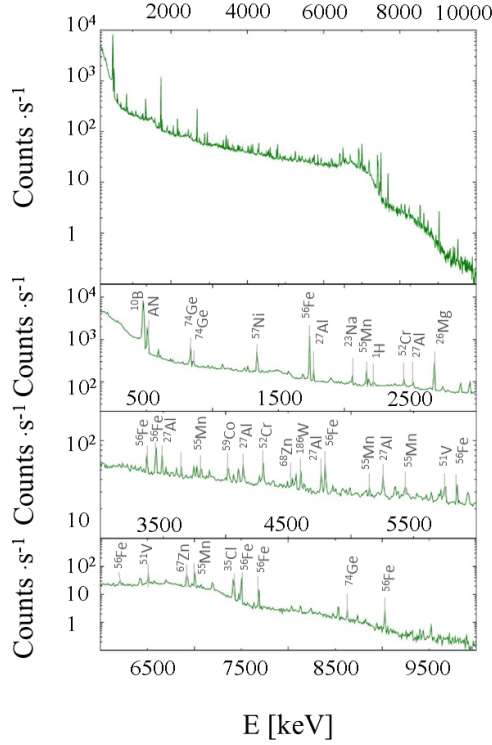


**Figure 2:** Prompt  $\gamma$ -ray spectrum recorded at IMAT beamline. The three lower panels provide the expanded views of the entire spectrum.

The analysis is performed using a combination of two software applications: ORIGIN-Lab [20] and ROOT [21,22]. Figures are obtained using GLE-Graphics [23]. Chemical elements identification is carried out through the comparison of two  $\gamma$  activation databases, i.e. Belgia et al. [7] and the International Atomic Energy Agency [24], both including delayed  $\gamma$ -rays. Additional check is performed evaluating the relative intensity of the  $\gamma$ -ray lines for the same element. Table 1 lists the identified  $\gamma$ -ray lines in the IMAT beamline at the position of the imaging based CCD detector without the camera box installed (configuration C1) and reported in figure 1 (b)). The value of the energy peak corresponds to the experimental peak centroid.  $\gamma$  line energies are compared to previous studies performed on VESUVIO and INES beamlines at Target Station 1 (TS-1) [1]. Same peaks identified in the three beamlines are labeled with an asterisk in Table 1. A semi-quantitative analysis was performed normalizing the peak area by the  $\gamma$  cross section ( $s_\gamma$ ) and the  $b(n,\gamma)$  cross section ( $\sigma_{(n,\gamma)}$ ) weighed by the absolute flux measured on IMAT beamline [25]. The relative percentages reported in table 1 are obtained for each element's  $\gamma$  line with the higher  $\gamma$  cross-section and through the normalization respect to the most intense (the  $^{57}\text{Fe}$  line at the  $\gamma$  energy of 1725.2 keV).

**Table 1.** IMAT  $\gamma$ -ray lines. \*Elements recorded on IMAT at TS2, VESUVIO and INES at TS1. Processes = (A) activation, (AN) annihilation, (C) neutron capture, (IS) inelastic scattering. Highest cross-section peak for each detected element are reported in bold, and the relative percentage (%) column reported the normalized percentage of peaks with respect to the most intense (the  $^{57}\text{Fe}$  at the  $\gamma$  energy of 1725.2 keV). The Notes column reports the peak energy from databases [(a) = [7], (b) = [24]]

Energy (keV)	Element	Process	Relative %	Notes (keV)
124.7	$^{51}\text{V}$			125.1 (b)
198.5*	$^{71\text{m}}\text{Ge}$	A		198.5
212.3*	$^{55}\text{Mn}$	C		212.0 (a)
<b>476.6*</b>	<b><math>^{10}\text{B}</math></b>	<b>(n, <math>\alpha</math>)</b>	<b>1.67</b>	<b>477.6 (a)</b>
509.8*		AN		511.0
<b>595.8*</b>	<b><math>^{73}\text{Ge}</math></b>	<b>C</b>	<b>14.30</b>	<b>595.8 (b)</b>
608.3*	$^{73}\text{Ge}$	IS		608.3 (b)
<b>749.0*</b>	<b><math>^{50}\text{Cr}</math></b>	<b>C</b>	<b>0.06</b>	<b>749.0 (b)</b>
<b>845.4*</b>	<b><math>^{55}\text{Mn}</math></b>	<b>A</b>	<b>0.03</b>	<b>846.7 (a)</b>
980.0*	$^{27}\text{Al}$	C		982.9 (b)
1173.5*	$^{118}\text{Sn}$	C		1173.2 (b)
1203.4*	$^{73}\text{Ge}$	C		1204.2 (b)
1258.9	$^{56}\text{Fe}$			1260.5 (b)
1292.3*	$^{116}\text{In, Sn}$	A, C		1293.5 (b)
<b>1434.3*</b>	<b><math>^{51}\text{V}</math></b>	<b>A</b>	<b>0.08</b>	<b>1434.1 (b)</b>
<b>1502.0</b>	<b><math>^{60}\text{Co}</math></b>		<b>0.65</b>	<b>1502.0 (b)</b>
1612.2*	$^{57}\text{Fe}$	C		1612.9 (b)
<b>1725.2*</b>	<b><math>^{56}\text{Fe}</math></b>	<b>C</b>	<b>100.00</b>	<b>1725.3 (b)</b>
<b>1776.6*</b>	<b><math>^{27}\text{Al}</math></b>	<b>A</b>	<b>51.51</b>	<b>1778.9 (a)</b>
2024.6	$^{23}\text{Na}$			2025.1 (b)
2110.6*	$^{55}\text{Mn}$	A		2112.6 (b)
2223.5*	<b><math>^1\text{H}</math></b>	<b>C</b>		<b>2223.3 (b)</b>
2238.3*	$^{53}\text{Cr}$	C		2239.1 (a)
2280.8	$^{27}\text{Al}$			2282.8 (a)
3053.0	$^{26}\text{Mg}$			3054.0 (b)
3413.6*	$^{57}\text{Fe}$	C		3413.1 (b)
3436.7*	$^{56}\text{Fe}$	C		3436.7 (a)
3463.5	$^{27}\text{Al}$			3464.9 (a)
<b>4026.3</b>	<b><math>^{59}\text{Co}</math></b>		<b>0.11</b>	<b>4022.6 (a)</b>
4058.5	$^{157}\text{Gd}$			4058.5 (b)
4132.4*	$^{27}\text{Al}$	C		4133.4 (a)
4217.4*	$^{57}\text{Fe}$	C		4218.6 (a)
<b>4321.5</b>	<b><math>^{52}\text{Cr}</math></b>		<b>3.46</b>	<b>4322.1 (a)</b>
<b>4574.5</b>	<b><math>^{186}\text{W}</math></b>		<b>0.14</b>	<b>4575.0 (b)</b>
4732.0	$^{27}\text{Al}$			4733.8 (a)
4807.8	$^{56}\text{Fe}$			4810.0 (a)
5253.3	$^{55}\text{Mn}$			5254.0 (a)
5752.0	$^{51}\text{V}$			5752.1 (b)
5921.0*	$^{56}\text{Fe}$	C		5920.4 (b)
6017.6*	$^{56}\text{Fe}$	C		6018.5 (b)
6429.8	$^{55}\text{Mn}$			6430.0 (a)
6517.4	$^{51}\text{V}$			6517.3 (b)
<b>6910.8</b>	<b><math>^{67}\text{Zn}</math></b>		<b>11.01</b>	<b>6911.0 (a)</b>
6929.3	$^{55}\text{Mn}$			6929.2 (b)
<b>7020.0</b>	<b><math>^{75}\text{As}</math></b>		<b>0.08</b>	<b>7020.1 (a)</b>
7212.4*	$^{27}\text{Al}$	C		7212.8 (a)
<b>7413.5</b>	<b><math>^{35}\text{Cl}</math></b>		<b>0.01</b>	<b>7414.0 (b)</b>
<b>7635.3</b>	<b><math>^{63}\text{Cu}</math></b>		<b>0.28</b>	<b>7637.4 (b)</b>
<b>8496.7</b>	<b><math>^{50}\text{Cr}</math></b>			<b>8498.4 (a)</b>
<b>9295.9*</b>	<b><math>^{54}\text{Fe}</math></b>	<b>C</b>	<b>6.43</b>	<b>9297.7 (b)</b>

The peak at 511 keV (blue colour in Table 1) is due to the electron–positron annihilation following pair production. This process occurs when  $\gamma$  with energies above 1022 keV are produced following neutron interactions with materials in the beamline. The 2224 keV hydrogen line (red colour in Table I) originates from the moderator materials, blockhouse walls and beam dump while the 478 keV  $^{10}\text{B}$  line from walls, beam dump, blades of sample “jaws” and slits and baffles in the flight tubes. The aluminum lines at 980 keV, 1777 keV, 2281 keV, 3463 keV, 4132 keV, 4732 keV and 7212 keV come from the CPS frame, upstream windows and flanges. The germanium peak at 198 keV, is due to the activation of the HPGe detector. The  $\gamma$ -ray lines at 749 keV, 2239 keV, and 4321 keV are from chromium; the 212 keV, 846 keV, 2112 keV, 5253 keV, 6530 keV and 6929 keV lines are from manganese. Chromium and manganese are elements composing the 6082-T6 and 2014-T6 aluminum alloys; the first one is used to manufacture the CPS frame and flanges, while the second one is used for the upstream windows. Chromium, manganese and copper, associated to the peak at 7637 keV are also present in the stainless steel used to manufacture the beam dump and walls. Cu is also present in the beam windows of inside the blockhouse. Peaks at 4429 keV and 6911 keV are from zinc, a component of 6082-T6 aluminum alloy. Peaks at 1259 keV, 1612 keV, 1725 keV, 3414 keV, 3437 keV, 4217 keV, 4808 keV, 5921 keV, 6018 keV, 7641 keV and 9296 keV are assigned to iron, abundant in the IMAT beamline and mainly present in the walls, upstream windows, beam dump and flanges. The 125 keV and 1434 keV lines are attributed to the vanadium present in the steel alloys and in the beam monitor; the 1502 keV and 4026 keV are identified as the activation of cobalt in the iron based materials.

In the C2 configuration,  $\gamma$  measurements are performed using the iron slab located at sample position and tilt  $45^\circ$  with respect to the beam direction.  $\gamma$  spectra with and without the iron slab are compared and reported in figure 3 (a). Both spectra are normalized to their integrated proton current and the acquisition live time. A distinct difference is visible in the region of  $4\text{--}9 \times 10^3$  keV. The presence of the iron slab at sample position leads to high radiation doses of high-energy  $\gamma$  rays (up to  $6 \cdot 10^3$  keV) due to the characteristic high intensity  $\gamma$  lines from iron. This kind of energy requires particular attention in order to provide appropriate shielding of the radiation sensitive components of the IMAT beamline. In the C3 configuration,  $\gamma$  measurements carried out with the vanadium rod at sample position are reported in figure 3 (b). This figure shows the prompt  $\gamma$ -ray energy contribution of the vanadium cylinder located in the sample position compared to the environmental  $\gamma$  background of the IMAT beamline. The vanadium measurements show a homogeneous counts enhancement overall the detected energy range as compared to the measurements recorded in C1. This result is due to the high intensity distribution of vanadium  $\gamma$  peaks all over the  $\gamma$  energy range; furthermore, the vanadium is a good isotropic scatterer and hence increases the fraction of scattered neutrons. The plots are normalized to the live-time to obtain comparable plots. The presence of the iron slab (details of the sample are reported in section 2) enhances the  $\gamma$  signal by 2% compared with the environmental  $\gamma$  background, while the vanadium rod (details of the sample are reported in section 2) produces a 59% increase. Although the dimensions of the two samples are not the same, the vanadium rod give the high contribution on the  $\gamma$  background due to the effects of the radiative absorption of the scattered neutrons on the walls.

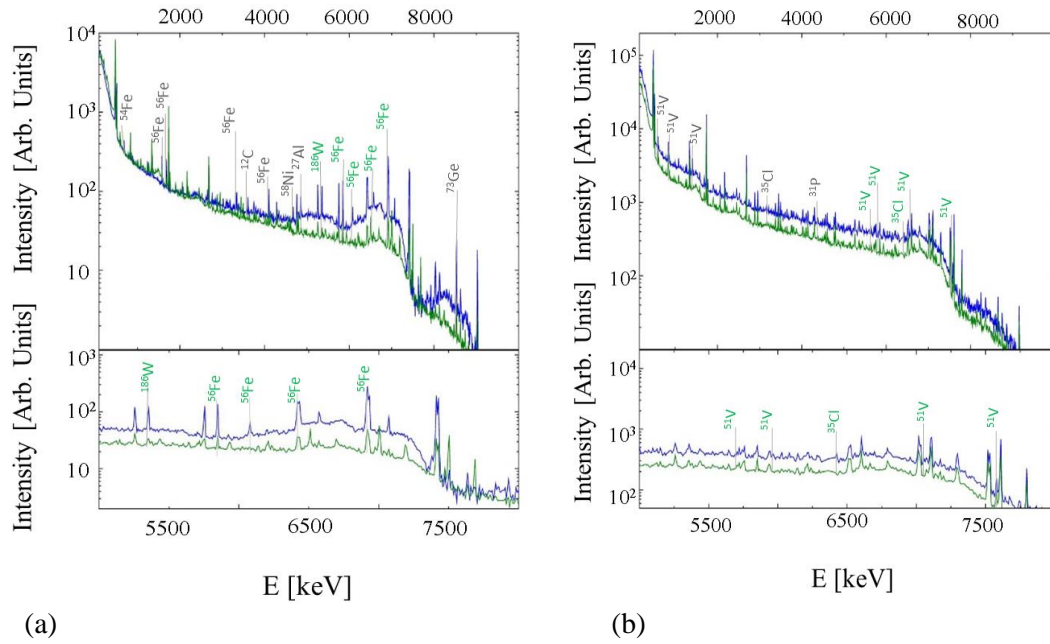


**Figure 3:** Prompt  $\gamma$ -ray spectra. (a) Configuration C2 with an iron slab at sample position (blue line) compared with the  $\gamma$  spectrum of IMAT (green line) at ISIS. (b) Configuration C3 with Vanadium rod at sample position (blue line) is compared to the  $\gamma$  spectrum of IMAT (green line) at ISIS. The two lower panels provides an expanded view from  $5 \times 10^3$  keV to  $8 \times 10^3$  keV.

Finally, the environmental  $\gamma$  spectrum recorded on IMAT (TS2) is reported together with the  $\gamma$  spectra on INES and VESUVIO beamlines (TS1) measured previously [1]. The three beamline have differences in the incident neutron spectra and beamline's components. Recorded  $\gamma$  spectra are plotted in figure 4.

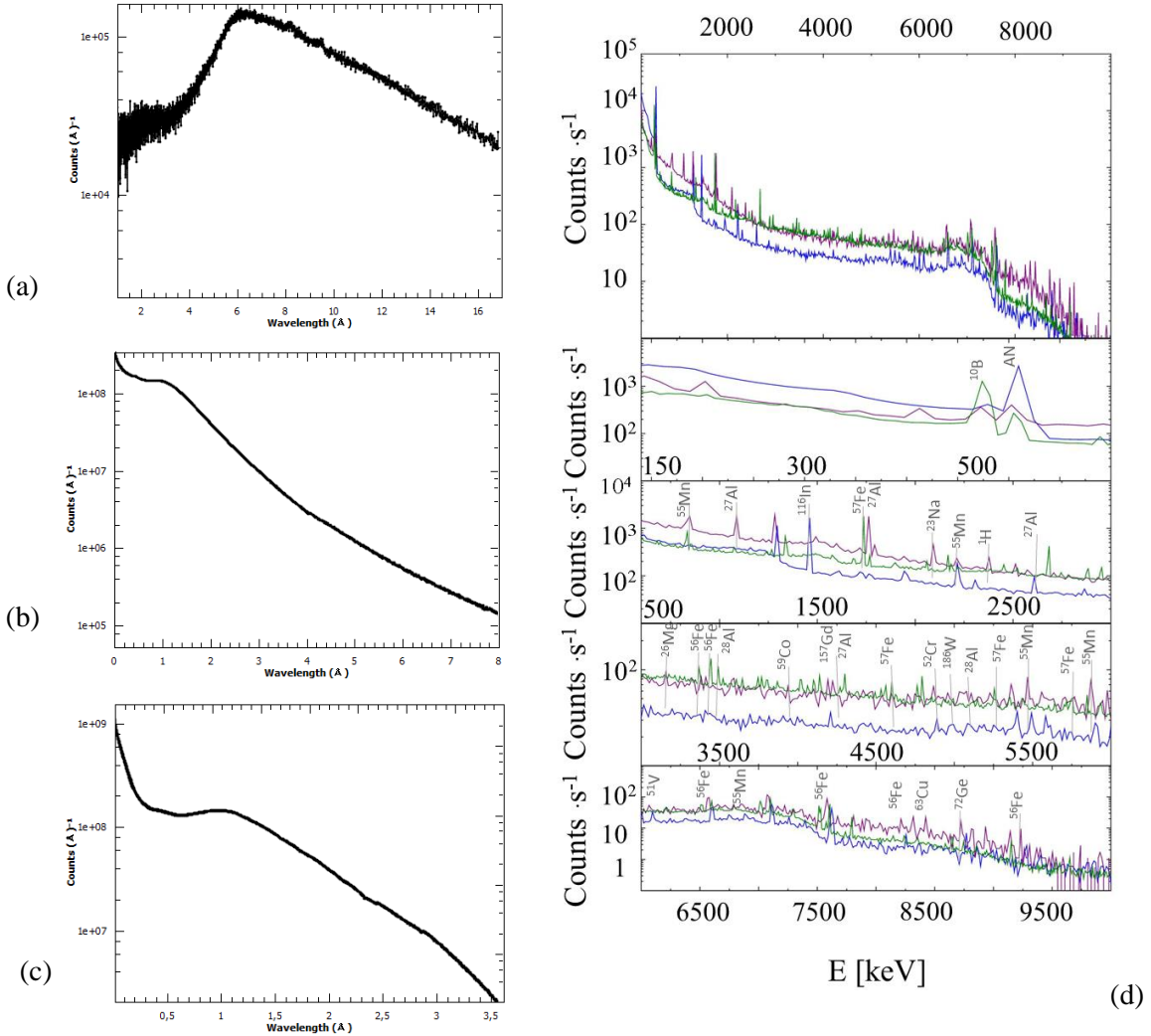


**Figure 4.** a) Incident neutron spectrum of IMAT beamline; b) Incident neutron spectrum of VESUVIO beamline; c) Incident neutron spectrum of INES beamline. d) Prompt  $\gamma$ -ray signal of IMAT beamline (green line), VESUVIO (violet line) and INES (blue line) beamlines at ISIS spallation neutron source.

These  $\gamma$  emissions are characterized by similar peaks for energies up to 2 MeV. The  $\gamma$  spectrum of IMAT shows differences all over the spectrum. These differences are attributed to the presence of 6082-T6 and 2014-T6 aluminum alloys along the neutron flight path due to the CPS frame, upstream windows, composition of the walls and beam dump. IMAT displays an intermediate trend compare with the INES and VESUVIO background. In the lower energy region [0-500] keV has a trend similar to the INES beamline; while in the energy region [500-1300] keV has the lowest  $\gamma$  signal of INES and VESUVIO. From [1300-9000] keV the IMAT  $\gamma$  background is intermediate between INES which is lower and the  $\gamma$  signal measured in the VESUVIO beamline which is higher. The headroom and volume of the experimental area have indeed an influence on the background absolute intensity, and its evaluation will be carried out by making use of Monte Carlo simulations. Further work will be devoted to the modeling of these background contributions, to provide indications for the optimization of the layout.

The last set of measurements are recorded in configuration C4 with the camera box located in place at 40

cm from sample position (see figure 1 (b)). These aim at the systematic study of the effects of environmental  $\gamma$ -signal on the camera components, i.e. on the detector (CCD/CMOS device). In such configuration, the tomographic camera box is placed facing the beam and part of the box is directly irradiated. A series of measurements are obtained by removing each component at the time, i.e neutron scintillator screen, scintillator frame, front upper and bottom shieldings of Boron10 painted Al-sheets, fused silica mirror, lens and finally the entire tomographic camera. The comparison of these series of spectra acquired for each configuration shows a systematic decrease of peaks and due to the removal of the camera components such as the aluminum box, silicon mirror, and  $^6\text{LiF/ZnS:Ag}$  scintillator. Results are reported in table 2.

**Table 2.** Configuration C4, IMAT  $\gamma$ -ray lines due to the tomographic camera box. The Notes column reports the peak energy from databases [(a) = [7], (b) = [24]]

E (keV)	Elements	Notes (keV)	
835.3	$^{53}\text{Cr}$	834.8	(b)
980.7	$^{27}\text{Al}$	982.9	(b)
1293.2	$^{115}\text{Sn}$	1293.6	(b)
1621.9	$^{27}\text{Al}$	1622.9	(b)
1829.9	$^{59}\text{Co}$	1830.8	(b)
1949.6	$^{35}\text{Cl}$	1951.2	(b)
2022.3	$^{59}\text{Co}$	2022.5	(a)
2031.1	$^7\text{Li}$	2032.3	(b)
2438.3	$^{25}\text{Mg}$	2438.5	(b)
2527.7	$^{19}\text{F}$	2529.2	(b)
2827.4	$^{24}\text{Mg}$	2828.2	(b)
2862.7	$^{32}\text{S}$	2863.8	(a)
3412.8	$^{24}\text{Mg}$	3413.1	(b)
3468.5	$^{186}\text{W}$	3469.4	(b)
3538.2	$^{28}\text{Si}$	3538.9	(b)
3830.9	$^{25}\text{Mg}$	3831.5	(b)
4247.1	$^{186}\text{W}$	4249.7	(b)
5013.7	$^{55}\text{Mn}$	5014.4	(b)
5100.1	$^{93}\text{Nb}$	5103.3	(b)
5473.9	$^{68}\text{Zn}$	5474.0	(b)
6988.5	$^{63}\text{Cu}$	6988.7	(b)
7056.8	$^{55}\text{Mn}$	7057.9	(b)
7722.2	$^{27}\text{Al}$	7724.0	(b)
7940.9	$^{52}\text{Cr}$	7938.5	(b)
8512.3	$^{50}\text{Cr}$	8510.8	(b)
9122.7	$^{67}\text{Zn}$	9120.1	(a)

Figure 5 shows the two configurations (with and without tomographic camera) and peak labeling due to the presence of the camera. Peaks reported in table 2 are labelled via the Molnar [4] and the IAEA database [24] definitions for  $\gamma$ -ray lines. The main contribution comes from the 7075-T6 aluminum in which zinc, magnesium and copper being the main elements; the mirror shows activation of silicon isotopes (i.e.  $^{28}\text{Si}$ ). The scintillator shows the activation of the silver contributing to the  $\gamma$  radiation dose.

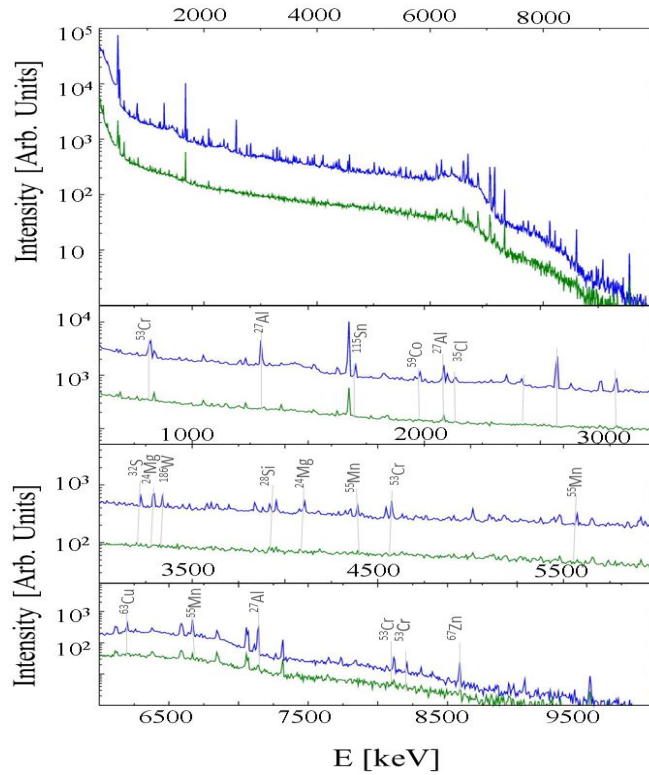


**Figure 5.** Configuration C4, Prompt  $\gamma$  spectra of the  $\gamma$  background with tomographic camera box in the beam (blue line) and without camera (green line) at IMAT beamline on TS2 at ISIS.

#### 4. Conclusions

The present study reports the characterization of the  $\gamma$ -ray signal of the IMAT beamline at TS-2 ISIS Spallation Neutron Source. These measurements provide specific information on the origin of the environmental  $\gamma$ 's produced during irradiation and the effects on the  $\gamma$  signal due to the presence of different samples.  $\gamma$  peaks are labelled and the main contributions are given by beamline layout elements present in the aluminum alloys, stainless steel and walls. The environmental  $\gamma$  spectrum recorded on two beamline at TS1 (INES and VESUVIO have a thermal/epithermal incident neutron beam) and one beamline at TS2 (IMAT that has a thermal incident neutron beam) are presented. The three measured gamma signal are completely different also due to the differences in the beamline's components. An estimation of the effects of the environmental  $\gamma$ -s due to the presence of the tomographic camera box in the beam (C4) shows that the camera produces a significant change in the  $\gamma$  spectra at the imaging detector position (CCD, CMOS etc.). In this context, other classes of materials used in nuclear fusion and high-neutron fluxes environment would potentially lead to a reduction and optimization of the  $\gamma$  background. For example, Reduced Activation Ferritic/Martensitic Steel (RAFM) [26] is a potential candidate for a reduction of the prompt  $\gamma$  emission coming from the beamstop on IMAT, to maintain the structural stainless steel properties and the same time reduce the background emission. Finally, even an evaluation of metallic structural materials may be consider for the camera box. The gamma spectroscopy method at spallation neutron sources is expected to impact both on the characterization of  $\gamma$  signals at neutron beamlines operating at spallation neutron sources, such as ISIS and the European Spallation Source (ESS), currently under construction in Lund (Sweden) and on characterization of materials [27].

#### 5. Acknowledgements

This work was supported within the CNR-STFC Agreement 2014–2020 (No. 3420 2014-2020) concerning collaboration in scientific research at ISIS Spallation Neutron Source.

## 6. References

- [1] A. Miceli, G. Festa, R. Senesi, E. Perelli Cippo, L. Giacomelli, M. Tardocchi, A. Scherillo, E. Schooneveld, C. Frost, G. Gorini and C. Andreani, ‘Measurements of Gamma Background at Spallation Neutron Source Beamlines’, *Journal of Analytical Atomic Spectrometry*, 29, 1897 (2014).
- [2] D.D. DiJulio, N. Cherkashyna, J. Scherzinger, A. Khaplanov, D. Pfeiler, C. P. Cooper-Jensen, K. G. Fissum, K. Kanaki, O. Kirstein, G. Ehlers, F. X. Gallmeier, D.E. Hornbach, E.B. Iverson, R.J. Newby, R.J. Hall-Wilton, P.M. Bentley, Characterization of the radiation background at the Spallation Neutron Source; *Journal of Physics: Conference Series* 746 (2016) 012033
- [3] Zs Kasztovszky, W. A. Kockelmann, E. Perelli Cippo, G. Gorini, M. Tardocchi, Prompt gamma activation studies on archaeological objects at a pulsed neutron source, *IL NUOVO CIMENTO*, 31-2, 2008
- [4] G.L. Molnar, 2004 Handbook of Prompt Gamma Activation Analysis with neutron beams, Kluwer Academic Publishers
- [5] A. Foderaro, The elements of neutron interaction theory, the MIT press 1971
- [6] A. Vertes, S. Nagy, Z. Klencsar, ‘Handbook of Nuclear Chemistry’, Springer Reference (2011)
- [70] Révay, Z. and G. L. Molnár: Standardisation of the Prompt Gamma Activation Analysis method. *Radiochimica Acta* 91 (2003) 361-369
- [8] Logan R.A. Lang D.V. Radiation effects in semiconductors. *J. Appl. Phys.* V47:p.3587, 1987
- [9] Jeong M.U. et. al. Radiation Effects in Semiconductors. Gordon and Breac Publish. N.Y., page p.287, 1971
- [10] Tanimura, Yoshihiko, & Iida, Toshiyuki (1998). Radiation effects on CCD image sensors (KEK-PROC--98-4). Nakazawa, M. (Ed.). Japan
- [11] W. Kockelmann, SY. Zhanga, J.F. Kelleher, J.B. Nightingale, G. Burca, J.A. James, ‘IMAT – a new imaging and diffraction instrument at ISIS’, *Physics Procedia* 43, 100 – 110 (2013)
- [12] G. Burca, J.A. James, W. Kockelmann, M.E. Fitzpatrick et al., A new bridge technique for neutron tomography and diffraction measurements, *Nucl. Instr. Meth. A*, 651 (1), 229-235 (2011)
- [13] T. Minniti, W. Kockelmann, G. Burca, J.F. Kelleher, S. Kabra, S.Y. Zhang, D.E. Pooley, E.M. Schooneveld, Q. Mutamba, J. Sykora, N.J. Rhodes, F.M. Pouzols, J.B. Nightingale, F. Aliotta, L.M. Bonaccorsi, R. Ponterio, G. Salvato, S. Trusso, C. Vasi, A.S. Tremsind and G. Gorini ‘Materials analysis opportunities on the new neutron imaging facility IMAT@ISIS’, *JINST* 11, C03014(2016)
- [14] E.H. Lehmann, P. Vontobel, G. Frei, C. Brönnimann, *Nucl. Instr. and Meth. A* 531, 228 (2004).
- [15] P. Vontobel, E.H. Lehmann, R. Hassanein, G. Frei, *Physica B* 385–386, 475 (2006).
- [16] G. Festa, E. Perelli Cippo, D. Di Martino, R. Cattaneo, R. Senesi, C. Andreani, E. Schooneveld, W. Kockelmann, N. Rhodes, P. Kudejova, K. Biro, K. Duza, Z. Hajnal, G. Gorini. ‘Neutron Resonance Transmission Imaging for 3D elemental mapping at the ISIS spallation neutron source’, *Journal of Analytical Atomic Spectrometry*, 30 (2015), 745
- [17] A. Pietropaolo, G. Festa, F. Grazzi, E. Barzagli, A. Scherillo, E. M. Schooneveld. A multitask neutron beam line for spallation neutron sources, *Europhysics Letters*, 95, 48007 (2011)
- [18] G. Burca, J.A. James, W. Kockelmann, M.E. Fitzpatrick et al., A new bridge technique for neutron tomography and diffraction measurements, *Nucl. Instr. Meth. A*, 651 (1), 229-235 (2011)
- [19] <http://www.ortec-online.com/>
- [20] <http://www.originlab.com/>
- [21] R. Brun and F. Rademakers, Root – an object oriented data analysis framework, *Proceedings AIHENP'96 Workshop*, Lausanne, 1996, <http://root.cern.ch/>.
- [22] R. Brun and F. Rademakers, Root – an object oriented data analysis framework, *Nucl. Instrum. Meth. Phys. Res. A*, 1997, 389, 81.
- [23] <http://www.gle-graphics.org/>
- [24] IAEA, International Atomic Energy Agency, Database for Prompt Gamma-ray Neutron Activation Analysis, 2013.
- [25] T. Minniti, K. Watanabe, G. Burca, D. Pooley, W. Kockelmann, Characterization of the new imaging and materials science facility IMAT, NIMA, in preparation.
- [26] B. van der Schaaf, F. Tavassoli, C. Fazio, E. Rigal, E. Diegele, R. Lindau, G. LeMarois, The development of EUROFER reduced activation steel, *Fusion Engineering and Design*, 69, 1–4, 197–203 (2003)
- [27] G. Festa, L. Arcidiacono, A. Pappalardo, T. Minniti, C. Cazzaniga, A.Scherillo, C. Andreani and R. Senesi. Isotope identification capabilities using time resolved prompt gamma emission from epithermal neutrons, *Journal of Instrumentation*, 11, C03060, (2016).